Two prestack converted-wave migration algorithms for vertical transverse isotropy

Baoniu Han
Center for Wave Phenomena, Dept. of Geophysics, Colorado School of Mines

ABSTRACT

Because the Earth's subsurface is generally anisotropic, data processing techniques that take anisotropy into account are required when the magnitude of anisotropy is so large that it cannot be ignored. Also, with ocean bottom seismic (OBS) data, in some cases converted-wave sections may be superior to conventional P-wave data. Here, I present two 2D algorithms for prestack depth migration of converted-wave data in transversely isotropic media with a vertical symmetry axis (VTI). Derived from the isotropic phase-shift-plus-interpolation (PSPI) and implicit finite-difference (FD) methods, these two algorithms inherit the accuracy of these wavefield-extrapolation migration methods. Based on an analytic solution of the Christoffel equation, the anisotropic PSPI algorithm can handle arbitrary magnitude of anisotropic parameters. The anisotropic FD algorithm, however, employs the weak-anisotropy assumption and thus is less accurate when anisotropy is strong. On the other hand, the anisotropic PSPI algorithm lacks the flexibility to deal with rapid spatial variation in the Thomsen parameters ϵ and δ unless the reference wavefield is computed for each pair of parameters. The anisotropic FD algorithm, however, can handle rapid variations of Thomsen parameters because each of the localized finite-difference operators is a function of the local parameters. Examples of migration on modeled data with these two converted-wave algorithms, for VTI media with moderate strength of anisotropy, show improved imaging results when both mode conversion and anisotropy are taken into account.

Key words: Converted wave, Finite difference, Phase shift, Depth migration.

Introduction

Conventional seismic data processing techniques are based on the assumption of isotropy. Such an assumption works fine when anisotropy is negligible; ignoring anisotropy, however, may lead to migration errors, especially in imaging dipping reflectors, as studied by Larner & Cohen (1993) and Jaramillo & Larner (1995) for both poststack and prestack migration. To obtain a focused and correctly positioned subsurface image, conventional isotropic algorithms need to be extended to accommodate anisotropy.

In recent years, multicomponent OBS data have shown, for certain situations, better quality than that of pure P-P data. Granli et al. (1999) show an example of imaging through a gas cloud with marine converted-wave data. Although the conventional isotropic, converted-wave data processing used in their example enhanced the imaging quality significantly over that of the P-P processing, anisotropy should be taken into account in areas that are strongly anisotropic. Thomsen (1999) shared his experience in the theoretical aspects of converted-wave data processing for heterogeneous, anisotropic media, indicating that converted-wave processing is more dependent on physical assumptions about rock velocities than is pure-mode processing.

Over the years, efforts have been made to develop P-wave migration algorithms for anisotropic media, especially for transverse isotropy. Kitchenside (1991) developed a phase-shift-based algorithm for TI media that used interpolation tables to link the horizontal

and vertical wavenumbers. Le Rousseau (1997) further used that idea for a table-driven PSPI (phase-shift-plus-interpolation) algorithm.

Other algorithms have been developed as well. Uzcategui (1994) extended the explicit downward-continuation method to TI media, using laterally-variant convolution operators that allow for lateral variation in both vertical velocity and anisotropy parameters. Ristow and Rühl (1997) developed an implicit finite-difference operator using the simplifying assumption of weak anisotropy.

The goal here is to develop 2D prestack, converted-wave (P-S) algorithms for depth migration in VTI media. Because prestack migration of common-shot (or common-receiver) gathers involves separate one-way propagation of source and receiver wavefields, for imaging converted waves all we need to do is pure-mode processing for each of the wavefields. That is, we can propagate one wavefield with the P-wave velocity, and the other with the SV-wave velocity. In the meantime, the same algorithm can be readily modified to process P-P data and S-P data because of the separate pure-mode wave-propagation feature.

For implementation, I turned to wavefield-extrapolation techniques, which are capable of generating an accurate image for complicated geological models. Another advantage with wavefield-extrapolation methods is that they can handle the triplication (caustics) of SV-wave naturally, while the ray-theoretical methods will encounter difficulty. Among such methods, I selected the phase-shift-plus-interpolation (PSPI) and implicit finite-difference (FD) methods as candidates mainly because I can use their P-wave anisotropic algorithms as the starting point for my implementations of converted-wave algorithms.

Here, I first review some background about isotropic PSPI and implicit FD algorithms, and about P- and SV-wave anisotropy. Then I describe the two anisotropic 2D prestack, converted-wave migration algorithms and test them on simple synthetic data.

Isotropic Algorithms

Phase-shift-plus-interpolation migration (PSPI)

Before addressing anisotropy, let us first review the basic PSPI approach, which is used here to develop an anisotropic depth-migration algorithm.

Given a homogeneous or $v(z)$ velocity field, in the frequency-wavenumber domain the 2-D acoustic wave equation is given by

$$k_x^2 P - \frac{\partial^2 P}{\partial z^2} = \frac{\omega^2}{v^2} P, \tag{1}$$

where P is the pressure wavefield, z is the depth, ω is the circular frequency and v is the velocity, assumed to be independent of x. Also k_x is the wavenumber in the lateral (i.e., x-) direction. Taking the spatial Fourier transform in the z-direction gives the dispersion relationship

$$k_x^2 + k_z^2 = \frac{\omega^2}{v^2}, \tag{2}$$

or

$$k_z = \pm\sqrt{\frac{\omega^2}{v^2} - k_x^2}, \tag{3}$$

and its corresponding one-way wave equation,

$$\frac{\partial P}{\partial z} = \pm i k_z P. \tag{4}$$

Here the $\pm$ signs correspond to the down and upgoing wavefields, respectively. Assuming that $v(z)$ is constant over the depth interval dz, analytic solutions of this one-way wave equation are

$$P(z + dz, k_x, \omega) = P(z, k_x, \omega) \exp^{\pm i k_z dz}. \tag{5}$$

Thus, wavefield extrapolation over the interval dz involves just a simple phase shift in the frequency-wavenumber domain.

This formula provides the foundation of the phase-shift migration method often called Gazdag migration (Gazdag, 1978). Advantages of this method are that it is stable, with no special requirement for the grid spacing, and it is accurate for dips up to 90°. Given these advantages, people have attempted to extend it to depth migration, in order to handle lateral velocity variation in a $v(x, z)$ medium.

When the velocity field is laterally varying, the pure phase-shift migration method fails because it requires computation in the spatial wavenumber domain. Gazdag and Sguazzero (1984) offered a method to treat lateral velocity variation that uses the main features of the phase-shift method. Instead of using a single velocity at each depth step, they used several reference velocities to account for the lateral velocity variation. At each depth step, the wavefield is propagated in the (ω,k_x) domain, each time with a different reference velocity, yielding multiple reference wavefields. Then, an inverse Fourier transform brings these reference wavefields back to the (ω,x) domain. The true wavefield is obtained by linearly interpolating the reference wavefields using the relationship between the local velocity and the reference velocities.

Implicit ω-x finite-difference migration (FD)

Since Clearbout (1985) developed it in the early 1970s, the FD method has been extensively used in seismic

imaging. Unlike the phase-shift migration method, the FD method works in the frequency-space domain, thus making it suitable to handle lateral velocity variation. In deriving the FD method, one starts again from the one-way acoustic wave equation (4) in the frequency-wavenumber domain, then substitutes $-i\partial x$ (where ∂x is the partial derivative with respect to x) for k_x, and approximates the square-root appearing in k_z with continued fractions. The resulting approximation of the one-way wave equation is solved by finite differences. Here I use an implicit (as opposed to the less costly explicit) finite-difference scheme because of its unconditional stability.

P-wave and *SV*-wave anisotropy

Since migration deals mostly with kinematic aspects of wavefield propagation, I will describe the anisotropic dispersion relationship and phase velocities for *P*- and *SV*-waves in VTI media.

Similar to the isotropic case, we have the anisotropic dispersion relationship,

$$k_z = \pm\sqrt{\frac{\omega^2}{v(\theta)^2} - k_x^2}, \tag{6}$$

where ω is the frequency, v is the angle-dependent velocity, θ is the phase angle with the symmetry axis, and k_x and k_z are horizontal and vertical wavenumbers. This relationship differs from that for the isotropic case in that velocity v is no longer a constant at any location (x, z); rather it depends on θ, the phase angle with respect to the symmetry axis in the transversely isotropic medium.

For all phase-shift-based migration algorithms, k_x is known; the issue is how to relate k_z to k_x. In the isotropic case, ω and v are constants, so k_z can be readily computed from k_x, ω, and v using the isotropic dispersion relationship. For anisotropic media, the angle-dependence of velocity makes the computation more complicated.

According to Tsvankin (1996), the phase velocity for *P*- and *SV*-waves can be written in terms of ϵ, δ, and the vertical *P*- and *SV*-wave velocities V_{P0} and V_{S0}, as

$$\frac{V^2(\theta)}{V_{P0}^2} = 1 + \epsilon\sin^2\theta - f/2 \pm f/2\sqrt{\left(1 + \frac{2\epsilon\sin^2\theta}{f}\right)^2 - \frac{2(\epsilon-\delta)\sin^2 2\theta}{f}}, \tag{7}$$

where the $+$ and $-$ signs are for the *P*- and *SV*-waves respectively, and

$$f \equiv 1 - V_{S0}^2/V_{P0}^2. \tag{8}$$

Expression (7) is obtained by solving for phase velocity as the eigenvalue of the Christoffel equation,

$$(a_{ijkl}n_j n_k - \delta_{il}V^2)U_i = 0, \tag{9}$$

where a_{ijkl} is the density-normalized stiffness tensor; n_j is the component of the unit vector in the slowness direction, and δ_{il} is the Kronecker symbolic delta. For the 2D problem studied here, each index takes two values — 1 and 3.

With the weak-anisotropic assumption, the expression for the anisotropic phase velocity can be simplified by expanding it to first order in the small parameters ϵ and δ:

$$\frac{V_p^2(\theta)}{V_{P0}^2} = 1 + 2\delta\sin^2\theta\cos^2\theta + 2\epsilon\sin^4\theta, \tag{10}$$

and

$$\frac{V_s^2(\theta)}{V_{S0}^2} = 1 + 2\sigma\sin^2\theta\cos^2\theta, \tag{11}$$

where $\sigma \equiv \frac{V_{P0}^2}{V_{S0}^2}(\epsilon - \delta)$.

Implementation of anisotropic converted-wave migration

1. PSPI algorithm

Using equation (7) as the starting point, Le Rousseau (1997) developed an anisotropic PSPI algorithm for P-P migration wherein he precomputes a table of $k_z(\theta)$ and $k_x(\theta)$ for supplied sets of anisotropic parameters, locates (interpolates) a given input k_x in the table, and finds the corresponding k_z. The accuracy of this table-driven algorithm is directly related to the size of the table; the finer the increment in θ and the more sets of reference anisotropic parameters, the better the results. With a large table, however, searching becomes time-consuming. Also, since the code runs in parallel mode across a network, transferring a large table to all the slave processors puts a heavy burden on the network.

In contrast to the above PSPI algorithm, I derived my algorithm directly from the Christoffel equation. With $p_j = n_j/V$, the Christoffel equation can be rewritten as

$$(a_{ijkl}p_j p_k - \delta_{il})U_i = 0, \tag{12}$$

where p_1 is the horizontal slowness, and p_3 is the vertical slowness ($p_2 = 0$).

The solution, $p_3(p_1)$, for both *P*- and *SV*-waves can be obtained simultaneously by solving the quadratic equation

$$Det[a_{ijkl}p_j p_k - \delta_{il}] = 0. \quad (13)$$

Also, since $p_1 = k_x/\omega$ and $p_3 = k_z/\omega$, k_x and k_z are connected through the relationship $p_3(p_1)$.

With the analytic solution for the Christoffel equation in VTI media, no interpolation table is needed. Also, I make no assumption about the strength of anisotropy and do not use the weak-anisotropy assumption.

As in the isotropic PSPI algorithm, several sets of reference parameters must be used for the migration. Ideally, reference wavefields would be generated for each set of reference parameters, but if, for example, we used five reference values for each of the four Thomsen parameters V_{P0}, V_{S0}, ϵ, and δ, 625 different sets of reference parameters would be required. To make the computation affordable, I make an assumption about the relationships among the parameters. It is assumed that all four Thomsen parameters have related lateral variation. Thus, if we pick n reference V_{P0}, we will also have the same number of reference parameters for V_{S0}, ϵ, and δ, resulting in n sets of reference parameters. At each depth step, I scan the P-wave velocity profile with the statistical method introduced by Bagaini et al. (1995) to determine the reference P-wave velocities, then choose reference values for SV-wave velocity, ϵ, and δ that are tied to the reference values of the P-wave velocity. Clearly, this way of choosing reference parameters is just one of many possible choices, and there may be situations for which this approach will be inadequate. For anisotropic PSPI, balancing the computation cost and the number of reference parameters remains an unresolved issue. The same issue of treating independent lateral variation in all four Thomsen parameters exists for all anisotropic algorithms based on a phase-shift operation, and for the explicit downward-continuation method (Uzcategui, 1994) as well.

2. Implicit FD algorithm

Ristow and Rühl (1997) developed a P-wave implicit finite-difference algorithm wherein the coefficients of the one-way finite-difference operator are expressed as a combination of V_{P0}, V_{S0}, ϵ and δ in each local cell of the model, thus permitting variations in all four parameters. The analytic expression for the finite-difference operator is derived using Taylor-series expansions, but this approach requires the weak-anisotropy assumption. So in the anisotropic FD algorithm, we sacrifice accuracy for strong anisotropy to gain the flexibility of accommodating lateral variation in the Thomsen parameters.

Note that the explicit downward-continuation method (Uzcategui, 1994) does not require the assumption of weak anisotropy. To explain this, let us start with the frequency-wavenumber domain, in which the phase shift operator $\exp^{\pm ik_z dz}$ is approximated by a finite-length operator for a given normalized frequency (defined by $\omega \triangle x/v$, where $\triangle x$ is trace spacing), then inverse Fourier transform the operator back to the frequency-space domain. At each step of the wavefield extrapolation, such a finite-length operator is convolved with the input wavefield to obtain the wavefield at the next depth step. The above approach is the explicit downward-continuation method (often called the FX method). The explicit downward-continuation method differs fundamentally from the implicit finite-difference algorithm. Here, "explicit" means this method is an explicit convolution algorithm. It does not pertain to an explicit finite-difference approximation and, strictly, no finite-difference approximation is used in deriving this method. As far as the algorithm is concerned, it is much closer to the phase-shift method, or the PSPI algorithm when considering lateral velocity variation.

For anisotropic migration, we could compute the explicit operator for each set of Thomsen parameters using the analytic solution for the phase velocity [equation (10)] in the frequency-space domain, so the explicit migration approach would not need a weak-anisotropy assumption. However, this explicit downward-continuation method suffers from the same parameter-choice problem as that in the anisotropic PSPI method. Also, the operator length further limits the maximum dip that this approach can handle.

Under the weak-anisotropy assumption, all the SV-wave kinematic expressions can be obtained by simply replacing parameters in the P-wave formulas with the corresponding ones for SV-waves (Tsvankin, 1996). These substitutions are

$$V_{P0} \longrightarrow V_{S0} \quad (14)$$

$$\delta \longrightarrow \sigma \quad (15)$$

and

$$\epsilon \longrightarrow 0. \quad (16)$$

Synthetic Examples

I tested these two algorithms on two simple models. The first one is an anisotropic medium with both horizontal and dipping reflectors. The anisotropic codes were used to demonstrate that they can handle the moderate anisotropy of this model. I would also like to test the ability of the two algorithms to handle the lateral variation of

anisotropy parameters. However, due to the lack of appropriate anisotropic data at the time of this writing, I used an isotropic model with lateral velocity variation. By setting the anisotropic parameters ϵ and δ to zero, the anisotropic codes were used to perform isotropic P-S migration with lateral change in velocity.

1. Anisotropic P-S data from horizontal and dipping reflectors

I generated anisotropic prestack converted-wave data using a ray-theoretical method for the VTI media (Alkhalifah, 1993). The model used in the experiment is relatively simple, containing two horizontal and two dipping reflectors, with the dip about 27°. The anisotropy parameters are constant, with $V_{P0} = 1500$ m/s, $V_{S0} = 750$ m/s, $\epsilon = 0.2$, $\delta = 0.05$. The dimension of the model is 4 by 2 km; 21 shot gathers were generated with the source position starting at 1 km and ending at 3 km, spaced at 100-m apart; and the receiver spacing is 10 m. The maximum offset of the split-spread data ranges from 2 km (source in the middle) to 3 km (source at the left or right end).

The prestack converted-wave PSPI migration (stacked with 21 shot gathers), shown in Figure 1a, was performed with the exact anisotropy parameters. This excellent result can be used as a benchmark for comparison with other results. The isotropic PSPI migration, shown in Figure 1b, was obtained by setting ϵ and δ to zero in the anisotropic PSPI algorithm. Because the correct vertical velocities were used, the imaged depth is correct for the horizontal reflectors. In practice, however, the migrated depth will generally be incorrect because conventional velocity analysis does not yield the true vertical velocity (it gives the stacking velocity, which approximates the normal-moveout velocity, V_{NMO}). Because anisotropy is ignored for the migration shown in Figure 1b, the two dipping reflectors are both poorly imaged and mispositioned.

The anisotropic FD results are shown in Figure 2. Figure 2a was obtained using the same anisotropic parameters as in the anisotropic PSPI algorithm. Even though the reflectors are imaged at the correct location, the amplitude of the dipping reflectors is much weaker than that of the anisotropic PSPI result. For a model with ϵ reduced to 0.1 (the other parameters were unchanged), the anisotropic FD result (Figure 2b) shows much improved amplitude for the dipping reflectors. Both results are far better than that of isotropic migration.

In an attempt to understand the cause of the weakening of the sloping reflectors in Figure 2a, I generated Figures 3 and 4, for single-shot migrations with source positions at the center of the model (2 km) and at the leftmost source location (1 km). Results in Figure 3 exhibit the same amplitude weakening seen in the full prestack migrations, so the weakening cannot be attributed to mis-stacking that might arise when the weak-anisotropy assumption is violated. Even though it is based on the weak-anisotropy assumption, the FD algorithm has imaged the dipping portions of the reflector at the correct positions. Note that for a relatively large value of ϵ, not only is the amplitude of the dipping reflectors reduced, the section shows artifacts (the artifacts above the horizontal reflectors in Figure 3b and Figure 3c are due to inhomogeneous portions of the wavefield). In the FD algorithm, the approximation to the anisotropic dispersion relationship causes two forms of error — one involving kinematics (traveltime and image position), and the other involving dynamics (amplitude). The FD results for both ϵ values show the correct image positions, which suggests that the quality of the kinematics in the weak-anisotropy approximation is not largely dependent on the strength of anisotropy. It is therefore possible that the truncated Taylor series approximation fails to treat amplitudes properly when anisotropy is moderate to strong. More study is needed in order to better understand the amplitude action of the anisotropic FD algorithm.

The approximation to the anisotropic dispersion relationship essentially put a dip limitation on the FD algorithm (up to 45° for this FD implementation). In Figure 3b and Figure 3c, the left and right ends of the lower horizontal reflectors are poorly focused. They correspond to propagation at more than 60° from vertical. Figure 4 further shows the dip limitation of the FD algorithm. In homogeneous anisotropic media, the PSPI algorithm can handle dip up to 90°, it is thus able to image all the reflectors in this model with just the shot gather at left edge (1 km) of the model. The FD algorithm, however, misfocused almost all the reflectors because from the source to the leftmost end of the lower horizontal reflector, the smallest propagation angle is already 57°, for other portions of reflectors, the dips are even larger.

2. Isotropic P-S data with lateral variation in velocity

The second model (Figure 5) contains three isotropic layers separated by two reflectors, one sinusoidal and the other dipping, with a dip of 7°. For migration, 131 common-shot gathers were used, with 20-m shot spacing and 10-m receiver spacing. The sources are located between 1200 m and 3800 m.

Figures 6 and 7 show migration results with the exact velocity model. Both algorithms were able to image the reflectors, and the lateral velocity variation is han-

dled correctly, but we could not image the left and right ends of both reflectors (Figure 5) because the modeled data did not have enough illumination. Both the PSPI and FD results show quite consistent amplitude behavior, although they show difference in the phase of the imaged reflectors. This might be due to the approximation to the dispersion relationship and to the finite-difference approximation in the FD algorithm. Further research will be carried out to study the phase difference between these two results.

A well-known fact about the illumination coverage is illustrated in Figures 8-10, which show single-shot migrations (source located at 2500 m; all the data have the same offset range) of three different data modes — P-P, P-S, and S-P. According to the Snell's law, the P-S result should have the most broad illumination area, so PS-wave should image more of the reflectors than will other waves (Figure 8). The S-P result shows the most narrow lateral extent, indicating that the SP-wave images the portions of the reflectors nearer to the source (Figure 9). The P-P result (Figure 10) shows lateral illumination between that in SP- and PS-wave migrations.

Conclusions

Since both anisotropic converted-wave migration algorithms (PSPI and implicit FD) were derived from the isotropic wavefield extrapolation algorithms, they inherit many properties of the conventional isotropic algorithms. The anisotropic PSPI algorithm has an advantage in its ability to treat strong anisotropy. Analytic solution of the Christoffel equation is used in the PSPI algorithm; no approximation is made for either the dispersion relationship or the strength of anisotropy. In contrast, the FD algorithm is based on a Taylor-series expansion that approximates the dispersion relationship, and a weak-anisotropy assumption must be made in order to do the Taylor expansion.

The two algorithms handle the model parameters (Thomsen parameters V_{P0}, V_{S0}, ϵ, δ of VTI media) in different ways. The anisotropic PSPI algorithm is equivalent to a series of anisotropic phase-shift migrations. Although anisotropic phase-shift migration is an ideal choice for time imaging in VTI media, performing multiple migrations for all possible combinations of Thomsen parameters is too computationally costly. In the implementation of the PSPI algorithm, I use a simple scheme to limit the number of parameters: all four Thomsen parameters are assumed to have similar lateral variation. Other choices, such as manually picking the reference Thomsen parameters, could be used in the PSPI algorithm. The choice for sets of reference parameters should balance the computation cost against expected accuracy. In contrast, with its localized finite-difference operator the anisotropic FD algorithm, can use any local combination of Thomsen parameters. Similar to the isotropic algorithm upon which it is based, the most attractive feature of the anisotropic FD algorithm is its ability to handle the lateral variation in the medium parameters.

Thus, for models with strong anisotropy, the PSPI approach is preferred. In contrast, if the lateral variation of the anisotropy parameters is known to be strong, the FD method is a better choice.

Both algorithms can be readily extended to deal with 3D data and tilted TI media. Making use of the SU library and parallelized with PVM library, three separate slave codes have been developed to account for P-P, P-S and S-P migration. An additional master code controls the choice of which slave code to run.

Acknowledgments

Support for this work was provided by Totalfina. I especially thank Yves Le Stuff who suggested that I work on this research, providing me continuous suggestions and support.

References

Alkhalifah, T. 1993. Efficient synthetic seismograms for transversely isotropic media with constant velocity gradient. *CWP Report, Center for Wave Phenomena, Colorado School of Mines, CWP-137*, 39–62.

Bagaini, C., Bonomi, E., & Pieroni, E. 1995. Data parallel implementation of 3-D PSPI. *65th Ann. Internat. Mtg., Soc. Expl. Geophys., Expanded Abstracts*, 188–191.

Clearbout, J. F. 1985. *Imaging the Earth's interior.* Oxford, England: Blackwell Science Publishers.

Gazdag, J. 1978. Wave equation migration with the phase shift method. *Geophysics*, **43**, 1342–1351.

Gazdag, J., & Sguazzero, P. 1984. Migration of seismic data by phase shift plus interpolation. *Geophysics*, **49**(2), 124–131.

Granli, J. R., Arntsen, B., Sollid, A., & Hilde, E. 1999. Imaging through gas-filled sediments using marine shear-wave data. *Geophysics*, **64**(3), 668–677.

Jaramillo, H., & Larner, K. 1995. Prestack migration error in transversely isotropic media. *65th Ann. Internat. Mtg., Soc. Expl. Geophys., Expanded Abstracts*, 1204–1207.

Kitchenside, P. W. 1991. Phase shift-based migration for transverse isotropy. *61th Ann. Internat. Mtg., Soc. Expl. Geophys., Expanded Abstracts*, 993–996.

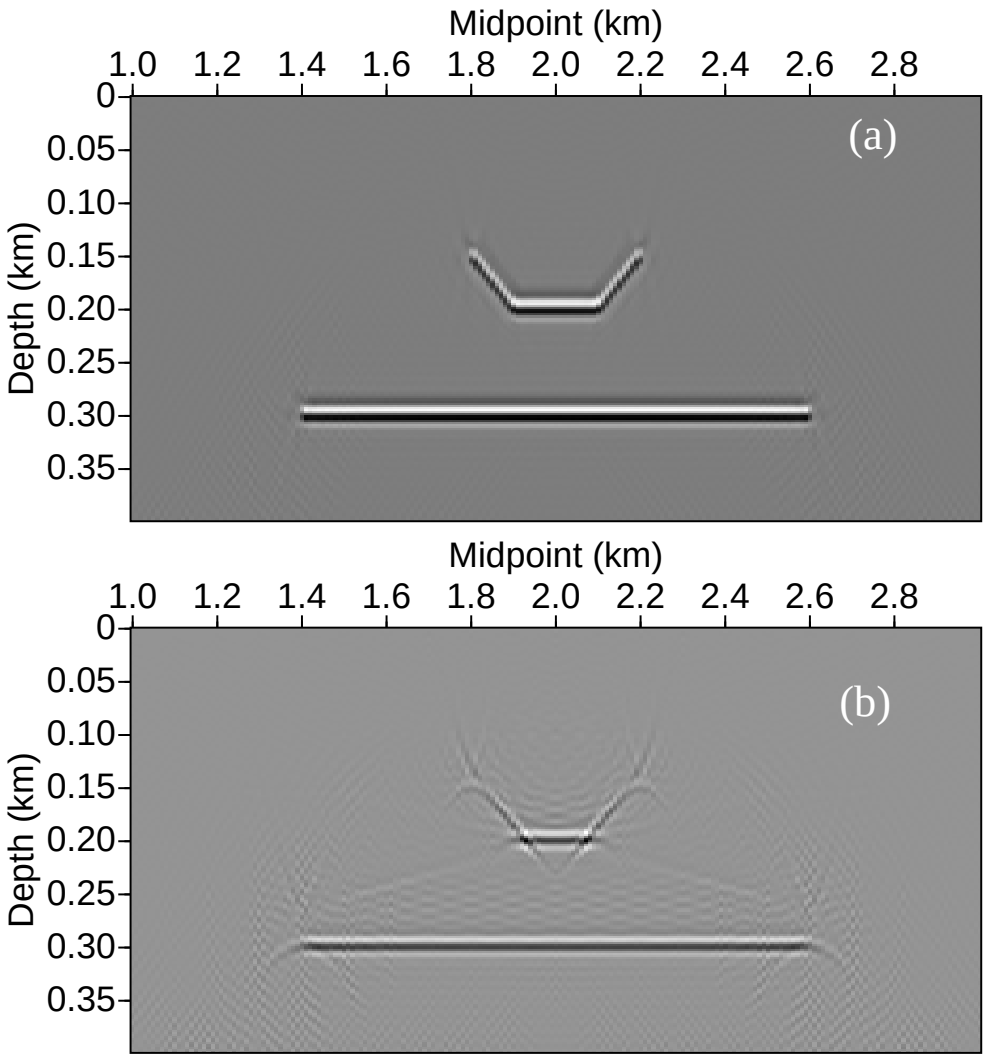

Figure 1. PSPI results; (a) anisotropic result using the exact parameters; (b) result with anisotropy ignored .

Larner, K., & Cohen, J. 1993. Migration error in factorized transversely isotropic media with linear velocity variation with depth. *Geophysics*, **58**, 1454–1467.

Le Rousseau, J. H. 1997. Depth migration in heterogeneous, transversely isotropic media with the phase-shift-plus-interpolation method. *67th Ann. Internat. Mtg., Soc. Expl. Geophys., Expanded Abstracts*, 1703–1706.

Ristow, D., & Rühl, T. 1997. Migration in transversely isotropic media using implicit operators. *67th Ann. Internat. Mtg., Soc. Expl. Geophys., Expanded Abstracts*, 1699–1702.

Thomsen, L. 1999. Converted-wave reflection seismology over inhomogeneous, anisotropic media. *Geophysics*, **64**(3), 678–690.

Tsvankin, I. 1996. P-wave signatures and notation for transversely isotropic media: An overview. *Geophysics*, **61**(2), 467–483.

Uzcategui, O. 1994. Depth migration in transversely isotropic media with explicit operators. *Ph.D. Thesis, CWP-163, Center for Wave Phenomena, Colorado School of Mines.*

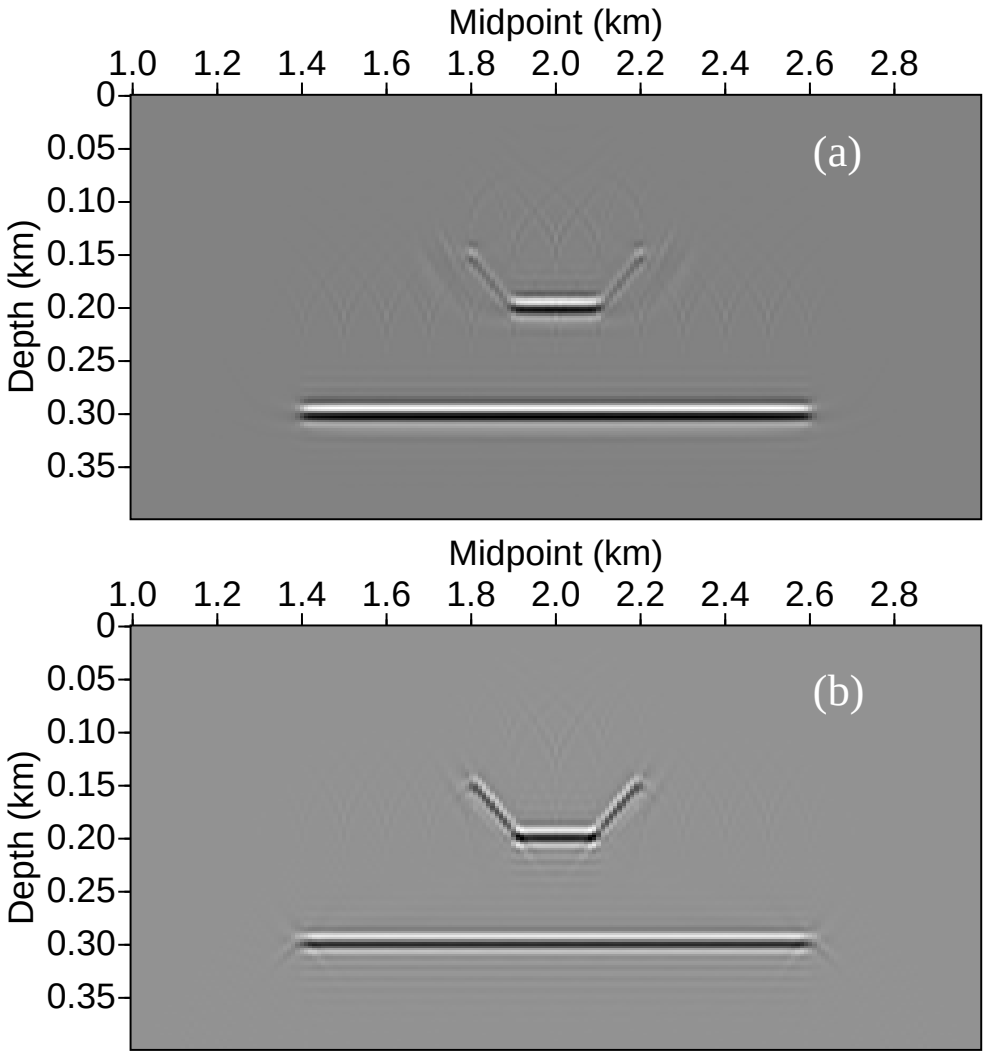

Figure 2. Anisotropic FD results: (a) FD result using the same parameters as in anisotropic PSPI; (b) FD result with ϵ reduced from 0.2 to 0.1, keeping other parameters untouched.

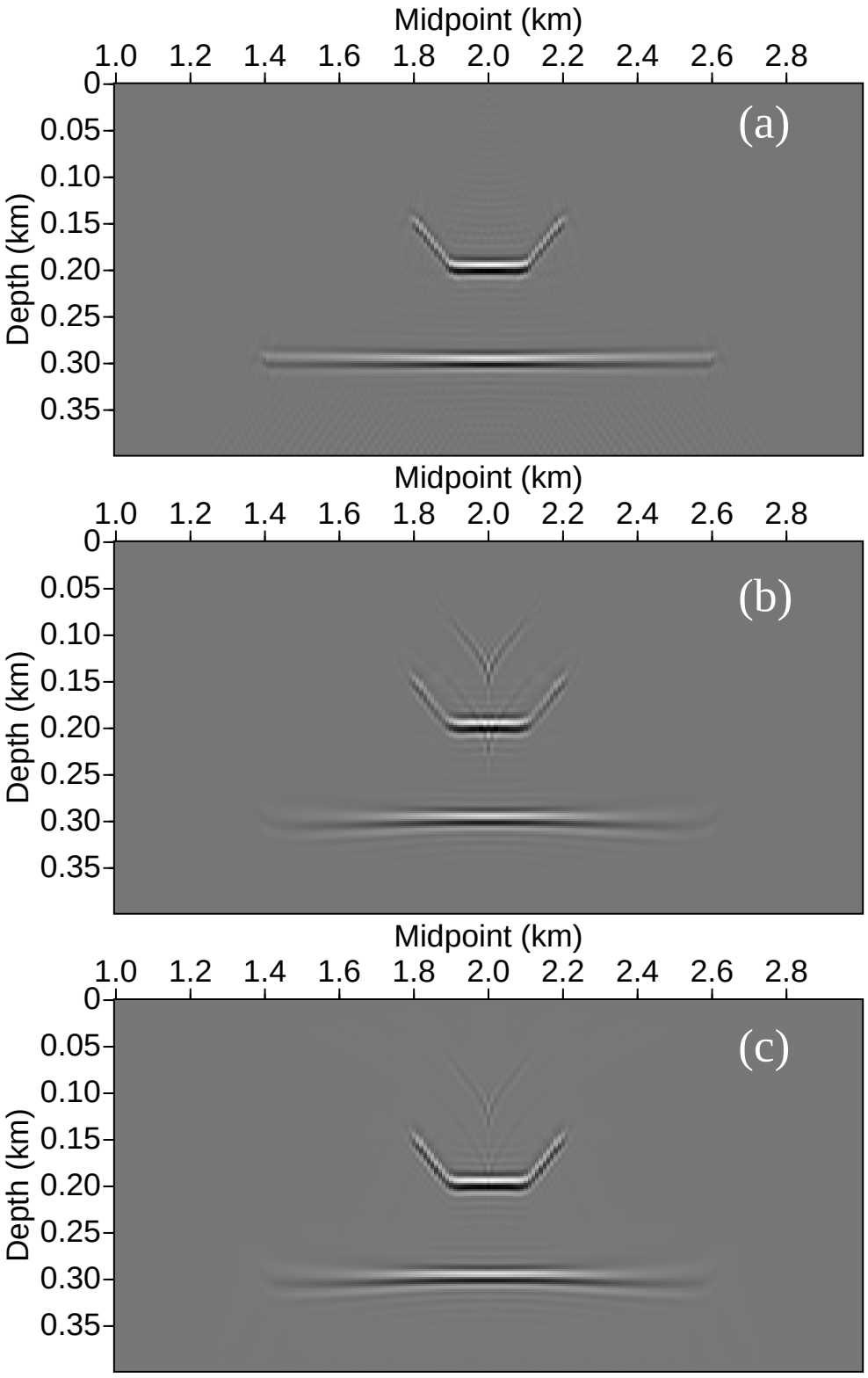

Figure 3. Migration of a single-shot gather with source at 2 km: (a) PSPI result; (b) FD result; (c) FD result with reduced ϵ value.

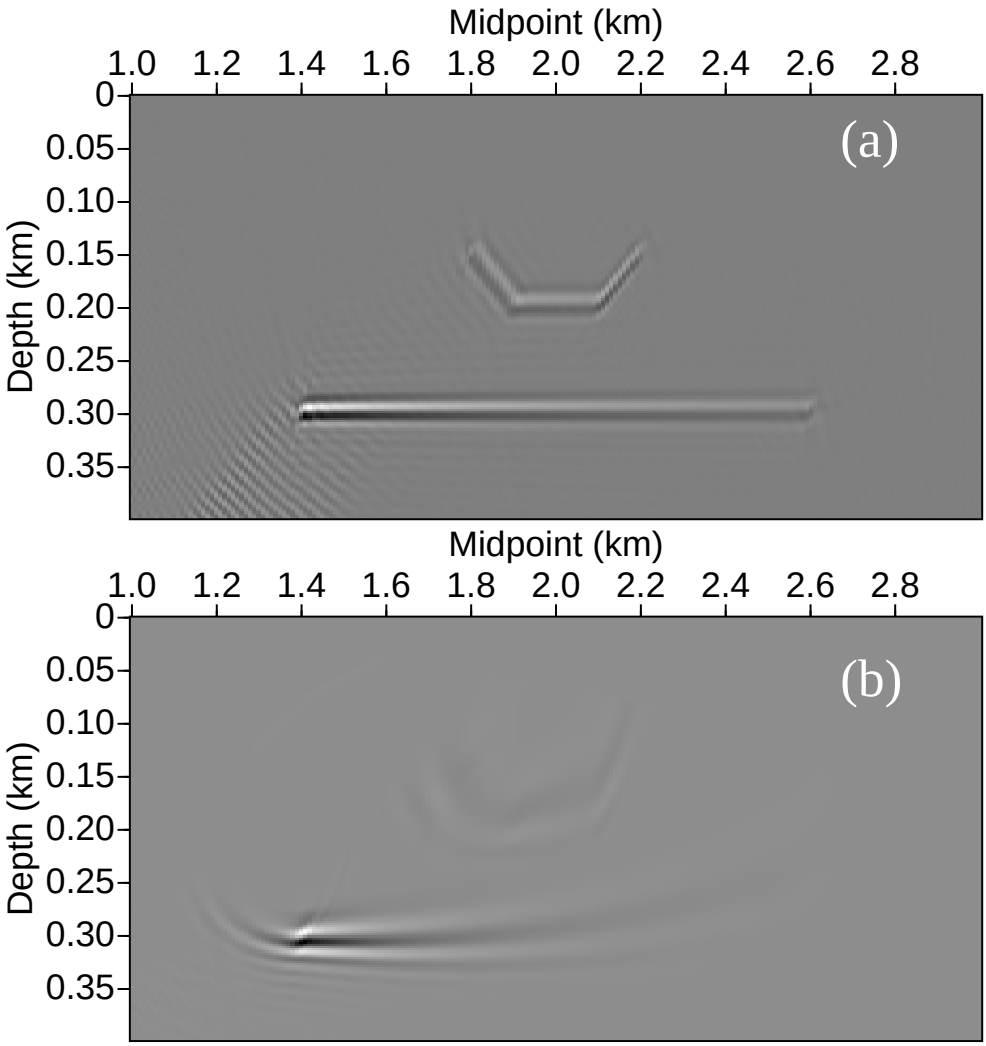

Figure 4. Migration of a single-shot gather with source at 1 km: (a) PSPI result; (b) FD result.

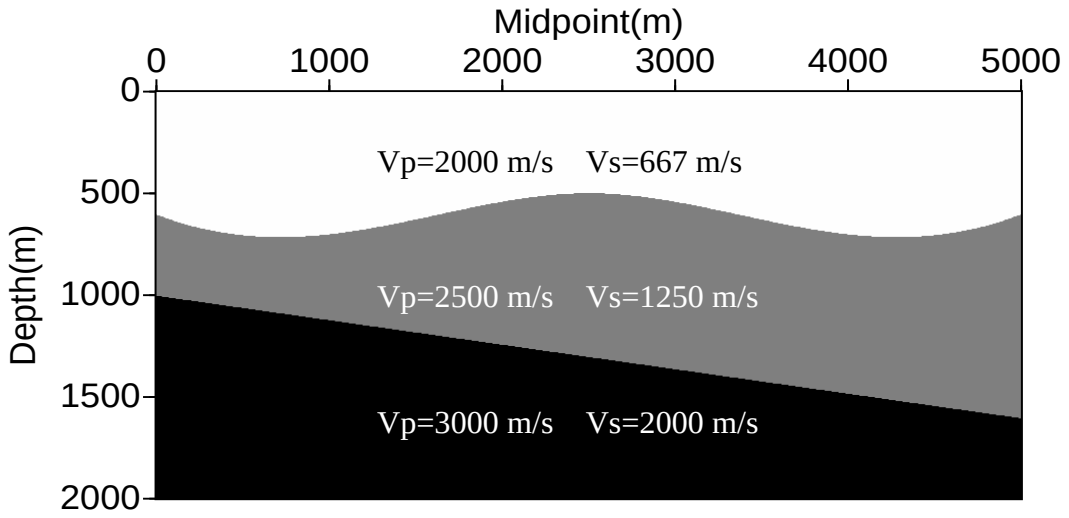

Figure 5. Velocity model for test 2

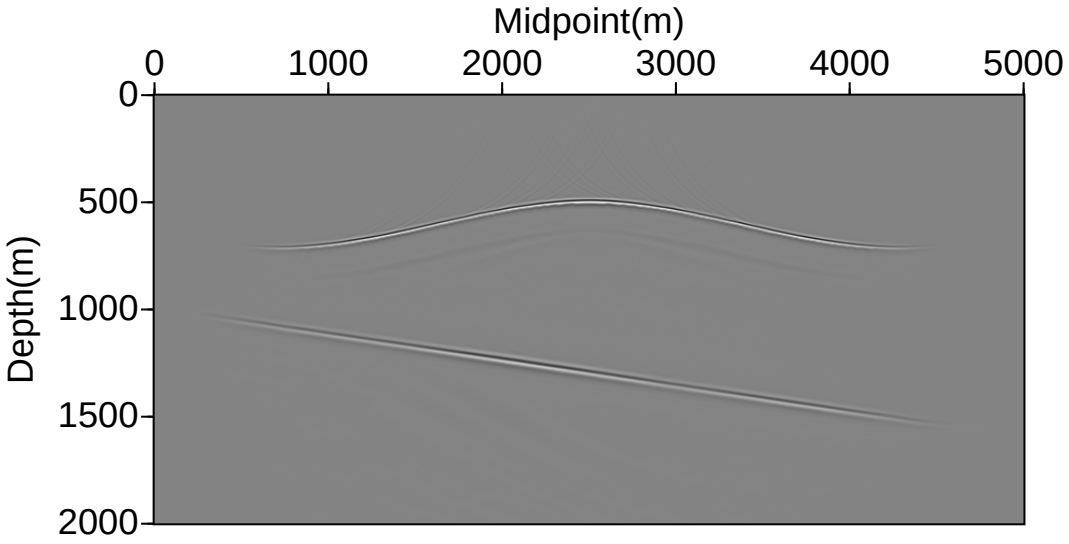

Figure 6. Prestack PSPI migration of *P*-*S* data with exact model.

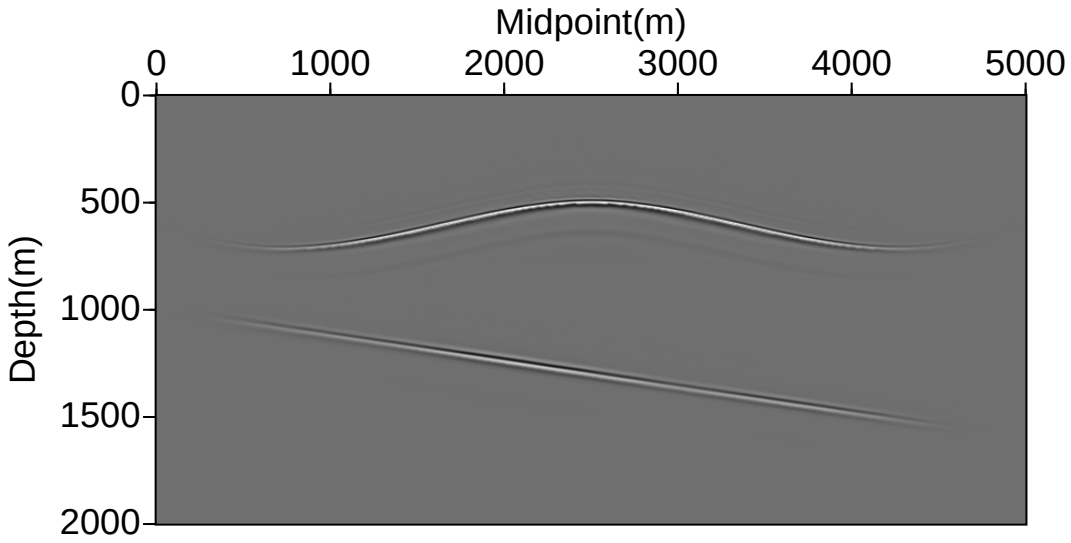

Figure 7. Prestack FD migration of P-S data with exact model.

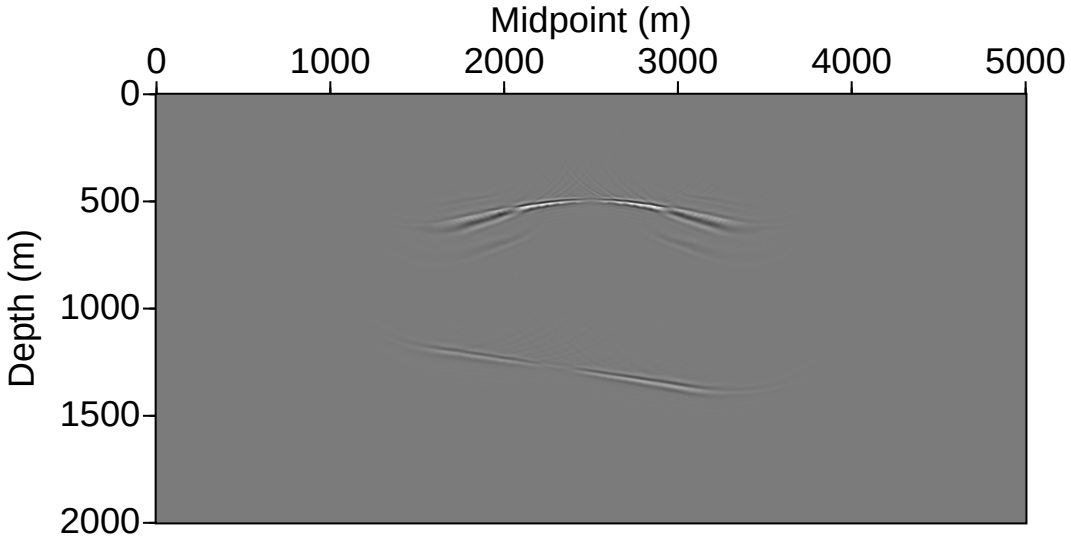

Figure 8. The single-shot FD migration of P-S data.

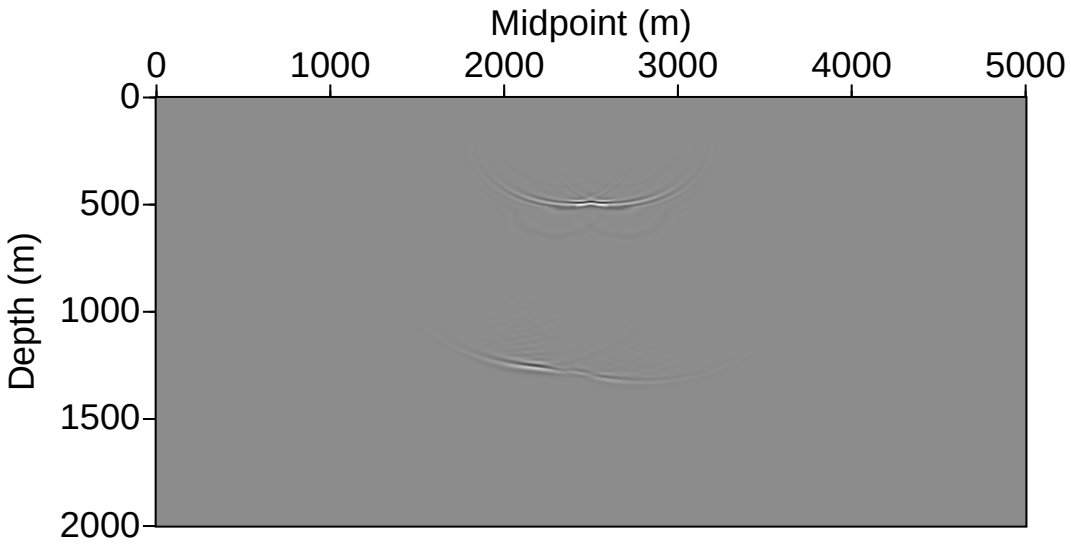

Figure 9. The single-shot FD migration of S-P data.

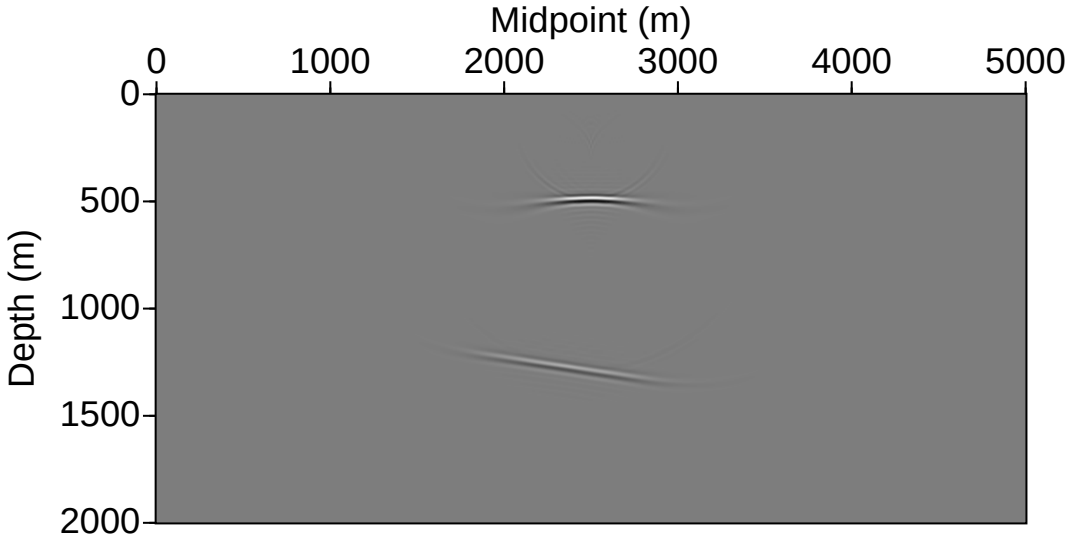

Figure 10. The single-shot FD migration of P-P data.